Letters

A Simple and Reconfigurable Wireless Power Transfer System With Constant Voltage and Constant Current Charging

Xingkui Mao, *Member, IEEE*, Jiayong Chen, *Student Member, IEEE*, Yiming Zhang, *Senior Member, IEEE*, and Jiqing Dong, *Member, IEEE*

***Abstract*—A typical charging profile for the Li-ion batteries in electric vehicles (EVs) includes a constant current (CC) charging stage and a constant voltage (CV) charging. This letter proposes a simple and reconfigurable topology for CC and CV outputs in an EV wireless charging system. The proposed system can be switched to series–series topology for CC output and inductor–capacitor–capacitor-series topology for CV output. Only one relay is introduced, unlike existing solutions where many passive components and relays are utilized for reconfiguration. Also, there is no need for frequency variation to achieve the shift of CC and CV. An experimental prototype is implemented to validate the proposal.**

***Index Terms*—Constant current (CC) charging, constant voltage (CV), inductor–capacitor–capacitor-series (*LCC*-S), reconfigurable, series–series (SS), wireless power transfer (WPT).**

I. Introduction

ELECTRIC vehicles (EVs) are developing rapidly as carbon emission can be reduced when replacing gasoline cars with EVs. The charging issue is one of the major technical issues concerning EVs. Wireless charging for EVs, enjoying the advantages of safety, convenience, automation, and freedom from human labor, has received enormous attention and become a research hotspot [1]. Li-ion batteries are widely used in EVs due to its high power density. A typical charging profile for Li-ion batteries includes constant current (CC) charging followed by constant voltage (CV) charging [2]. Thus, to comply with this profile, the wireless charging should have a CC output as well as a CV output.

In the current literatures, there are multiple ways to achieve CC and CV outputs. The first method is to switch the working frequencies to achieve CC and CV outputs at different working frequencies [3]–[6]. However, zero phase angle cannot be guaranteed at these two frequencies points, introducing extra reactive power. In addition, it is not easy to achieve the target within a limited working frequency such as from 79 to 90 kHz according to J2954 from Society of Automotive Engineers.

Another method is to switch topologies to suit for CC and CV charging [7]–[10], such as from the series–series (S–S) topology to the inductor–capacitor–capacitor-series (*LCC*-S) topology. In the current version using this method, many extra passive components like inductors and capacitors are introduced, or many relays are used for topology reconfiguration.

This letter proposes a novel topology to enable CC and CV outputs without introducing extra passive components. The three resonant loops in the *LCC*-S topology are employed to form the S–S topology. Only one relay is utilized. In this way, a simple and low-cost solution for CC and CV outputs is offered.

Manuscript received September 9, 2021; revised October 11, 2021; accepted October 13, 2021. Date of publication October 29, 2021; date of current version January 19, 2022. This work was supported by the National Natural Science Foundation of China under Grant 51207025. *(Corresponding author: Xingkui Mao.)*

The authors are with the College of Electrical Engineering and Automation, Fuzhou University, Fuzhou 350108, China (e-mail: mxk782@fzu.edu.cn; 2537992865@qq.com; zym@fzu.edu.cn; dongjiqing@fzu.edu.cn).

Color versions of one or more figures in this article are available at https://doi.org/10.1109/TPEL.2021.3123869.

Digital Object Identifier 10.1109/TPEL.2021.3123869

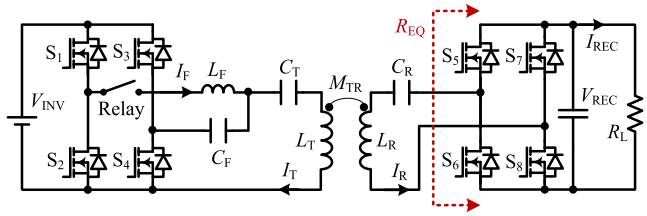

Fig. 1. Proposed topology for CC and CV outputs.

II. Proposed CC and CV Charging Topology

The proposed topology for CC and CV outputs is depicted in Fig. 1. L_{T} (L_{R}), C_{T} (C_{R}), and I_{T} (I_{R}) are the respective transmitter (receiver) self-inductance, series capacitance, and current. M_{TR} is the mutual inductance. L_{F} is the compensating inductance and C_{F} is the parallel capacitance. I_{F} is the current of L_{F}. V_{INV} is the inverter dc voltage. R_{L} is the load resistance. V_{REC} and I_{REC} are the charging voltage and current, respectively.

In the proposed topology, there are three resonant loops: Loop 1 consisting of L_{F} and C_{F}, Loop 2 consisting of C_{F}, C_{T}, and L_{T}, and Loop 3 consisting of L_{R} and C_{R}. Thus, the resonant frequency ω_0 equals

$$\omega_0 = \frac{1}{\sqrt{L_{\mathrm{F}}C_{\mathrm{F}}}} = \frac{1}{\sqrt{L_{\mathrm{F}}\frac{C_{\mathrm{F}}C_{\mathrm{T}}}{C_{\mathrm{F}}+C_{\mathrm{T}}}}} = \frac{1}{\sqrt{L_{\mathrm{R}}C_{\mathrm{R}}}}. \tag{1}$$

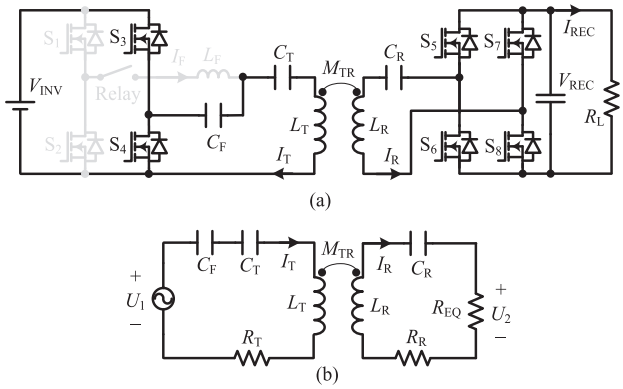

Fig. 2. Proposed system for CC output. (a) Topology. (b) Equivalent circuit.

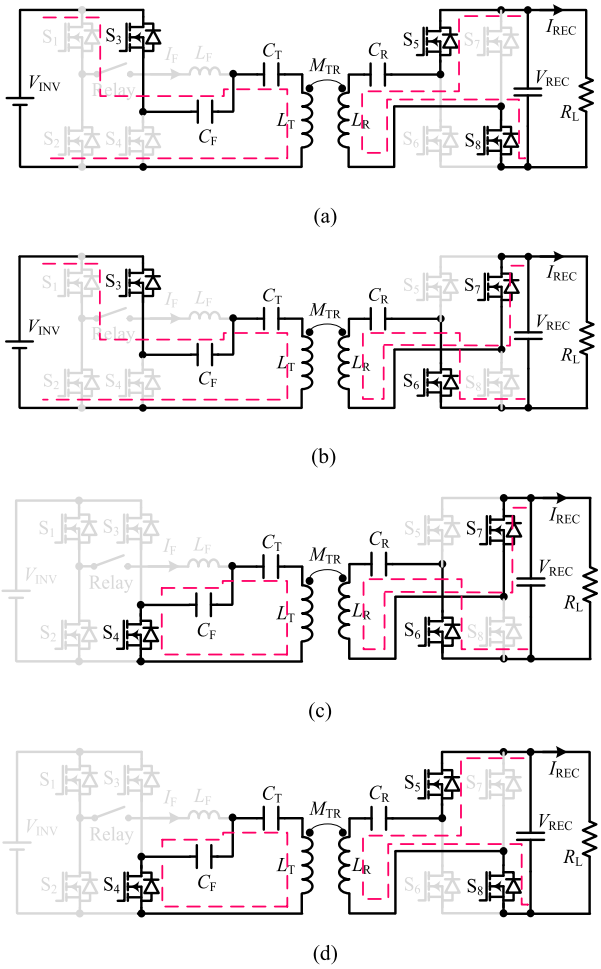

Fig. 3. Current flow paths at the CC mode. (a) With positive U_1 and positive U_2. (b) With positive U_1 and negative U_2. (c) With zero U_1 and negative U_2. (d) With zero U_1 and positive U_2.

The rectifier works at synchronous rectification. Thus, the equivalent ac load resistance R_{EQ} and the ac voltage of the

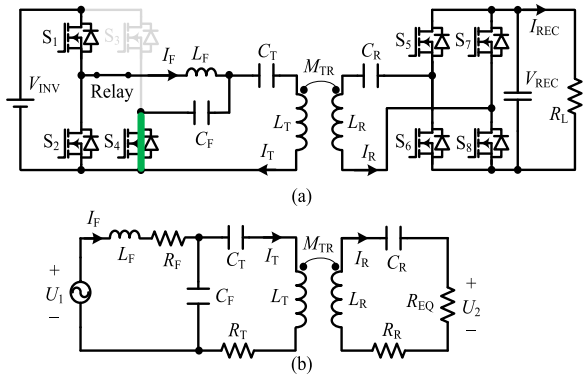

Fig. 4. Proposed system for CV output. (a) Topology. (b) Equivalent circuit.

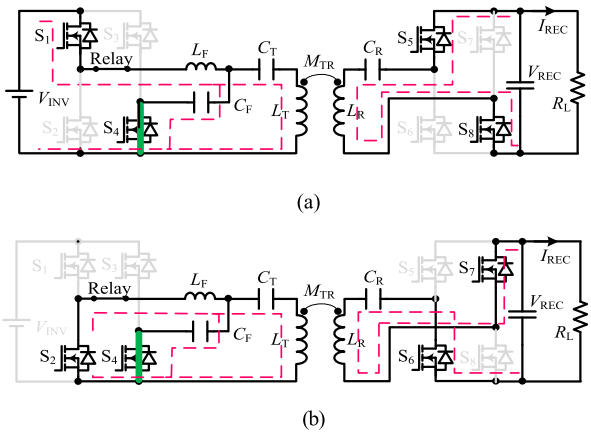

Fig. 5. Current flow paths at the CV mode. (a) With positive U_1 and positive U_2. (b) With zero U_1 and negative U_2.

rectifier U_2 can be expressed as

$$\begin{cases} R_{\mathrm{EQ}} = \frac{8}{\pi^2} R_{\mathrm{L}} \\ U_2 = \frac{2\sqrt{2}}{\pi} V_{\mathrm{REC}}. \end{cases} \tag{2}$$

A. CC Output

For CC output, the relay is OFF and an S–S topology driven by a half-bridge inverter is formed, as shown in Fig. 2(a). The equivalent circuit for CC output is shown in Fig. 2(b). R_{T} (R_{R}) is the equivalent resistance of the transmitter (receiver). U_1 is the equivalent ac voltage of the inverter. The phase-shift between U_1 and U_2 is controlled with 90° at the CC mode, then its current flow paths are shown in Fig. 3.

U_1 is expressed as

$$U_1 = \frac{\sqrt{2}}{\pi} V_{\mathrm{INV}}. \tag{3}$$

Based on the Kirchhoff voltage law (KVL) and ignoring R_{T} and R_{R}, we have

$$\begin{cases} I_{\mathrm{T}} = \frac{U_1 R_{\mathrm{EQ}}}{(\omega_0 M_{\mathrm{TR}})^2}, I_{\mathrm{R}} = \frac{U_1}{\omega_0 M_{\mathrm{TR}}} \\ U_2 = \frac{U_1 R_{\mathrm{EQ}}}{\omega_0 M_{\mathrm{TR}}}. \end{cases} \tag{4}$$

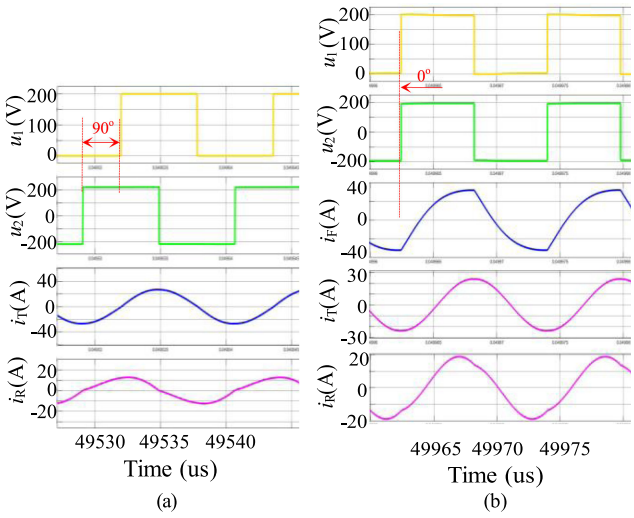

Fig. 6. Key simulation voltage and current waveforms. (a) CC output with $R_L = 28\ \Omega$. (b) CV output with $R_L = 28\ \Omega$.

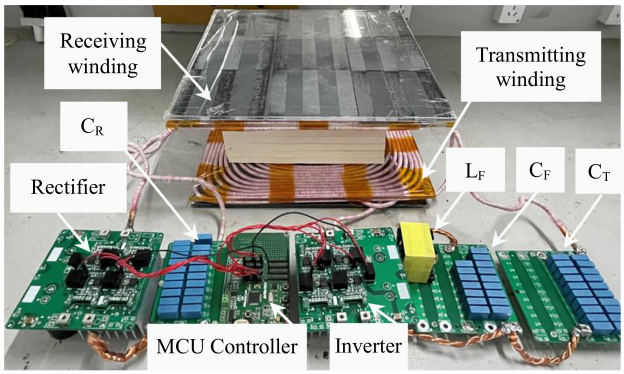

Fig. 7. Photograph of the experimental prototype.

Thus, the dc charging voltage and current are

$$I_{\mathrm{REC}} = \frac{4}{\pi^2}\frac{V_{\mathrm{INV}}}{\omega_0 M_{\mathrm{TR}}}, \quad V_{\mathrm{REC}} = \frac{4}{\pi^2}\frac{V_{\mathrm{INV}} R_{\mathrm{L}}}{\omega_0 M_{\mathrm{TR}}}. \tag{5}$$

Considering R_{T} and R_{R}, the ac–ac efficiency can be expressed as

$$\eta = \frac{I_{\mathrm{R}}^2 R_{\mathrm{EQ}}}{I_{\mathrm{R}}^2 R_{\mathrm{EQ}} + I_{\mathrm{T}}^2 R_{\mathrm{T}} + I_{\mathrm{R}}^2 R_{\mathrm{R}}} = \frac{1}{1 + \frac{R_{\mathrm{R}}}{R_{\mathrm{EQ}}} + \frac{R_{\mathrm{T}} R_{\mathrm{EQ}}}{(\omega_0 M_{\mathrm{TR}})^2}}. \tag{6}$$

The efficiency is maximized when

$$R_{\mathrm{EQ}} = \sqrt{\frac{R_{\mathrm{R}}}{R_{\mathrm{T}}}}\omega_0 M_{\mathrm{TR}}. \tag{7}$$

B. CV Output

For CV output, the relay and the switch S_4 are constantly ON while the switch S_3 is constantly OFF, forming an *LCC*-S topology driven by a half-bridge inverter, as shown in Fig. 4(a).

The equivalent circuit for CV output is shown in Fig. 4(b). R_{F} is the equivalent resistance of L_{F}. The phase-shift between U_1

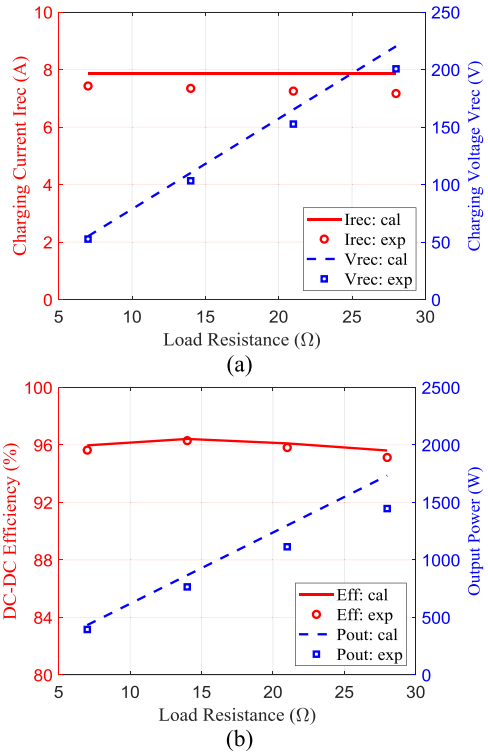

Fig. 8. Calculated and experimental results of CC output. (a) DC charging current I_{REC} and voltage V_{REC}. (b) DC–DC efficiency and output power.

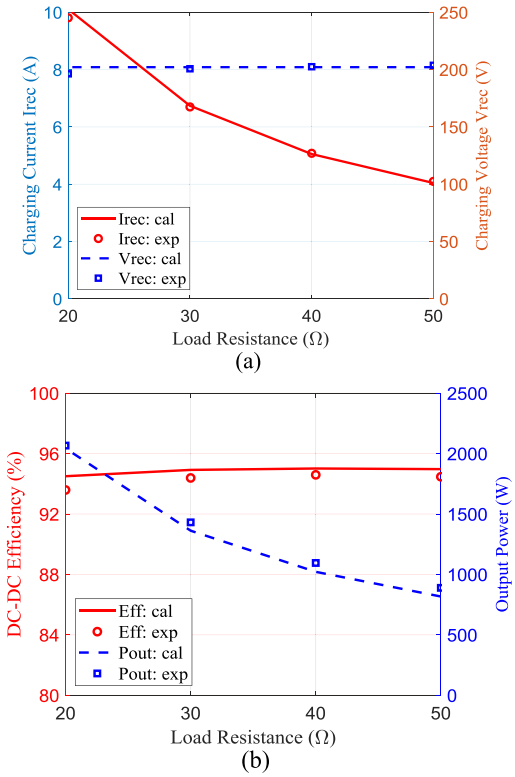

Fig. 9. Calculated and experimental results of CV output. (a) DC charging current I_{REC} and voltage V_{REC}. (b) DC–DC efficiency and output power.

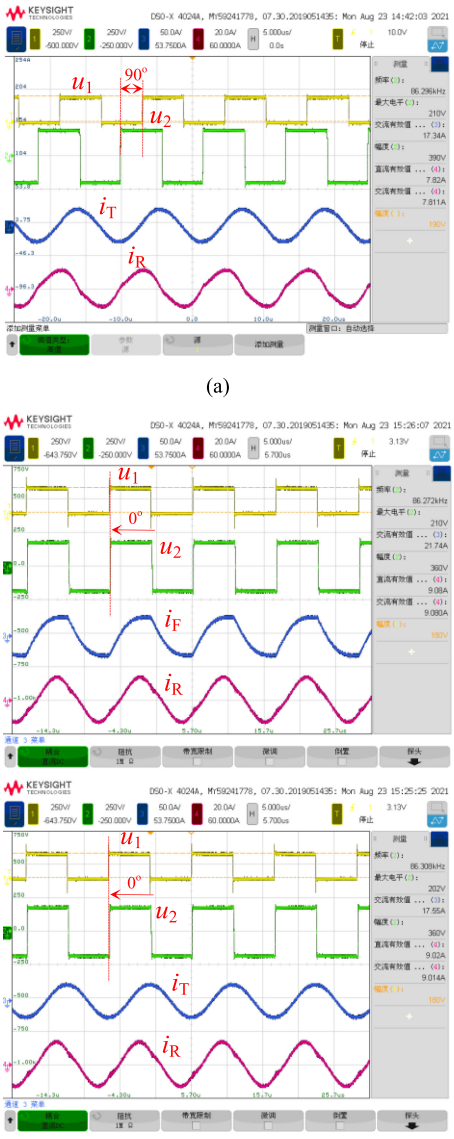

Fig. 10. Experimental waveforms. (a) CC output with load resistance $R_{\mathrm{L}} = 28\ \Omega$. (b) CV output with load resistance $R_{\mathrm{L}} = 28\ \Omega$.

and U_2 is controlled with the same phase at the CV mode, then its current flow paths are shown in Fig. 5.

Based on KVL and ignoring R_{F}, R_{T}, and R_{R}, we have

$$\begin{cases} I_{\mathrm{F}} = \left(\dfrac{M_{\mathrm{TR}}}{L_{\mathrm{F}}}\right)^2 \dfrac{U_1}{R_{\mathrm{EQ}}},\ I_{\mathrm{T}} = \dfrac{U_1}{\omega_0 L_{\mathrm{F}}} \\ I_{\mathrm{R}} = \dfrac{M_{\mathrm{TR}}}{L_{\mathrm{F}}} \dfrac{U_1}{R_{\mathrm{EQ}}},\ U_2 = \dfrac{M_{\mathrm{TR}}}{L_{\mathrm{F}}} U_1. \end{cases} \tag{8}$$

Thus, the dc charging voltage and current are

$$\begin{cases} I_{\mathrm{REC}} = \dfrac{1}{2} \dfrac{M_{\mathrm{TR}}}{L_{\mathrm{F}}} \dfrac{V_{\mathrm{INV}}}{R_{\mathrm{L}}} \\ V_{\mathrm{REC}} = \dfrac{1}{2} \dfrac{M_{\mathrm{TR}}}{L_{\mathrm{F}}} V_{\mathrm{INV}}. \end{cases} \tag{9}$$

Considering R_{F}, R_{T}, and R_{R}, the ac–ac efficiency can be expressed as

$$\eta = \frac{I_{\mathrm{R}}^2 R_{\mathrm{EQ}}}{I_{\mathrm{R}}^2 R_{\mathrm{EQ}} + I_{\mathrm{F}}^2 R_{\mathrm{F}} + I_{\mathrm{T}}^2 R_{\mathrm{T}} + I_{\mathrm{R}}^2 R_{\mathrm{R}}}$$

TABLE I
PARAMETERS OF SIMULATION AND EXPERIMENTAL PROTOTYPE

V_{INV} (V)	200	f (kHz)	86	M_{TR}(μH)	19.1
				k	0.251
L_{T} (μH)	76.0	L_{R} (μH)	76.0	L_{F} (μH)	9.4
C_{F} (nF)	360.1	C_{T} (nF)	52.4	C_{R} (nF)	45.1

$$= \frac{1}{1 + \dfrac{R_{\mathrm{R}}}{R_{\mathrm{EQ}}} + \dfrac{R_{\mathrm{T}} R_{\mathrm{EQ}}}{(\omega_0 M_{\mathrm{TR}})^2} + \left(\dfrac{M_{\mathrm{TR}}}{L_{\mathrm{F}}}\right)^2 \dfrac{R_{\mathrm{F}}}{R_{\mathrm{EQ}}}}. \tag{10}$$

The efficiency is maximized when

$$R_{\mathrm{EQ}} = \sqrt{\frac{R_{\mathrm{R}} + \left(\dfrac{M_{\mathrm{TR}}}{L_{\mathrm{F}}}\right)^2 R_{\mathrm{F}}}{R_{\mathrm{T}}}}\, \omega_0 M_{\mathrm{TR}}. \tag{11}$$

From (7) and (11), the optimal load resistance in the CC mode is smaller than the CV mode. This matches with the real value of load during CC–CV charging where the load resistance in the CC mode is smaller than in the CV mode.

III. Simulations and Experiments

Modeling and simulation of the prototype are carried out with MATLAB/Simulink, and the parameters are tabulated in Table I. The key simulation voltage and current waveforms are given in Fig. 6. An experimental prototype is implemented whose photo is depicted in Fig. 7.

The experimental results of the CC and CV outputs are shown in Figs. 8 and 9, respectively. CC and CV outputs have been achieved.

The experimental waveforms of both CC and CV outputs are depicted in Fig. 10. The experimental waveforms are consistent with the simulation.

IV. Conclusion

This letter proposed a simple and reconfigurable topology for CC and CV outputs in a wireless charging system. The *LCC*-S topology can be reconfigured to the S–S topology by using the three resonant loops. Unlike the existing solutions where many passive elements and relays are utilized, the proposed solution only adopts a relay, and no extra inductors or capacitors are introduced compared with the *LCC*-S topology. In addition, the system works at one single frequency, easily complying with existing standards. A prototype was developed. The experimental results validated the effectiveness of the proposed system.

References

[1] Y. Zhang, T. Kan, Z. Yan, Y. Mao, Z. Wu, and C. C. Mi, "Modeling and analysis of series-none compensation for wireless power transfer systems with a strong coupling," *IEEE Trans. Power Electron.*, vol. 34, no. 2, pp. 1209–1215, Feb. 2019.

[2] J. Lu, G. Zhu, D. Lin, Y. Zhang, J. Jiang, and C. C. Mi, "Unified load-independent ZPA analysis and design in CC and CV modes of higher order resonant circuits for WPT systems," *IEEE Trans. Transp. Electrific.*, vol. 5, no. 4, pp. 977–987, Dec. 2019.

[3] V. Vu, D. Tran, and W. Choi, "Implementation of the constant current and constant voltage charge of inductive power transfer systems with the double-sided LCC compensation topology for electric vehicle battery charge applications," *IEEE Trans. Power Electron.*, vol. 33, no. 9, pp. 7398–7410, Sep. 2018.

[4] L. Yang, X. Li, S. Liu, Z. Xu, and C. Cai, "Analysis and design of an LCCC/S-compensated WPT system with constant output characteristics for battery charging applications," *IEEE J. Emerg. Sel. Topics Power Electron.*, vol. 9, no. 1, pp. 1169–1180, Feb. 2020.

[5] Z. Huang, S. C. Wong, and C. K. Tse, "An inductive-power-transfer converter with high efficiency throughout battery charging process," *IEEE Trans. Power Electron.*, vol. 34, no. 10, pp. 10245–10255, Oct. 2019.

[6] W. Zhang, S. Wong, C. K. Tse, and Q. Chen, "Load-independent duality of current and voltage outputs of a series- or parallel-compensated inductive power transfer converter with optimized efficiency," *IEEE J. Emerg. Sel. Topics Power Electron.*, vol. 3, no. 1, pp. 137–146, Mar. 2015.

[7] Y. Chen, H. Zhang, S. Park, and D. Kim, "A switching hybrid LCC-S compensation topology for constant current/voltage EV wireless charging," *IEEE Access*, vol. 7, pp. 133924–133935, 2019.

[8] Y. Chen, B. Yang, Z. Kou, Z. He, G. Cao, and R. Mai, "Hybrid and reconfigurable IPT systems with high-misalignment tolerance for constant-current and constant-voltage battery charging," *IEEE Trans. Power Electron.*, vol. 33, no. 10, pp. 8259–8269, Oct. 2018.

[9] Y. Li *et al.*, "Reconfigurable intermediate resonant circuit based WPT system with load-independent constant output current and voltage for charging battery," *IEEE Trans. Power Electron.*, vol. 34, no. 3, pp. 1988–1992, Mar. 2019.

[10] X. Qu, H. Han, S. Wong, C. K. Tse, and W. Chen, "Hybrid IPT topologies with constant current or constant voltage output for battery charging applications," *IEEE Trans. Power Electron.*, vol. 30, no. 11, pp. 6329–6337, Nov. 2015.